

# Photoelectrochemical, Optical, and Dielectric Studies on Photoactive Assemblies Prepared from Silver Orthophosphate and 2,2 bithiophene in Thermoplastic Gel Electrolyte

Kasem K. Kasem\*, Heaven Power Douglas

Indiana University Kokomo, School of Sciences, Kokomo, IN, 46904

\*E-mail: [kkasem@iuk.edu](mailto:kkasem@iuk.edu)

Received: 9 September 2021 / Accepted: 26 October 2021 / Published: 4 July 2022

---

An n/p organic/inorganic interface [IOI] assembly consists of poly 2,2 bithiophene [PBTh] as a p-type semiconductor and silver orthophosphate [ $\text{Ag}_3\text{PO}_4$ ] were subjected to photoelectrochemical [PEC], optical, and electrochemical impedance spectroscopy [EIS] studies in thermoplastic gel electrolyte [TPGE], consisting of polyethylene glycol [PEG]/ $\text{I}_2/\text{I}^-$ . Optical studies show that the occlusion of  $\text{Ag}_3\text{PO}_4$  in PBTh created hybrid sub-bands with smaller band gaps between the highest occupied molecular orbitals [HOMO] and lowest unoccupied molecular orbitals [LUMO] of the host polymer. Studies also showed that the occlusion of  $\text{Ag}_3\text{PO}_4$  into PBTh matrix network increased the generated photocurrent and further prolonged the lifetime of photo-generated charges. EIS studies show that charge carrier transport takes place by hopping transport, which is consistent with the amorphous, non-crystalline nature of the studied assemblies. Both silver and phosphate ions contributed to the enhancement of the photo-activities of PBTh by doping of Ag atoms in PBTh, and phosphate anions prolonged the lifetime of photogenerated charges created in the surface layers. The assembly showed stability and resistance of photodegradation as evident from the regeneration of the same photoresponse after a longer period of operation.

---

**Keywords:** Photoelectrochemistry, Gel electrolyte, photoactive polymer, Silver Phosphate, Impedance studies.

## 1. INTRODUCTION

Using inorganic binary compounds such as metal oxides, and chalcogenides as photoactive materials were explored several decades ago. The studies were extended to cover some metal phosphates. In particular, n-type  $\text{Ag}_3\text{PO}_4$  [silver orthophosphate] that possesses a bandgap of 2.36 eV [1] was found to be a promising visible light photocatalyst due to its ability for photooxidation and generation of oxygen by water splitting in the presence of visible light [2]. Composites containing

$\text{Ag}_3\text{PO}_4$  were synthesized to improve the photodegradation efficiency and overcome the stability issue. Some of these composites include  $\text{SnO}_2/\text{Ag}_3\text{PO}_4$  [3],  $\text{TiO}_2/\text{Ag}_3\text{PO}_4$  [4],  $\text{AgX}/\text{Ag}_3\text{PO}_4$  [5],  $\text{Fe}_3\text{O}_4/\text{Ag}_3\text{PO}_4$  [6],  $\text{Ag}/\text{Ag}_3\text{PO}_4$  [7] and so on. Currently, carbon material/ $\text{Ag}_3\text{PO}_4$  nanocomposites [carbon quantum dot] [CQDs]/ $\text{Ag}_3\text{PO}_4$  [8], graphene/ $\text{Ag}_3\text{PO}_4$  [9], and CNT/ $\text{Ag}_3\text{PO}_4$  [10] have been used to improve the photodegradation efficiency and stability of  $\text{Ag}_3\text{PO}_4$ . Photoactive inorganic /organic interfaces were studied. Some of these studies included metal oxides and metal chalcogenides with some photoactive organic compounds [8-12].

The choice of an electrolyte can be an important factor in the stability of the photoactive substance. The use of polymer gel electrolytes can be a potential alternative to liquid electrolytes to avoid the disadvantage associated with the erosion of photoactive film assemblies in photoelectrochemical cell devices that use liquid electrolytes. Among these polymer gel, electrolytes are thermoplastic gel electrolytes [TPGE]. Several studies were focused on fabrication, working principle, and up-to-date status of DSSCs and batteries using polymer electrolytes [13-16].

We used  $\text{I}^-/\text{I}_3^-$  as the redox-active material in the proposed TPGE, due to several desirable [17-19] properties associate with  $\text{I}^-/\text{I}_3^-$  redox system. This includes good solubility, low absorption of light, suitable redox potential, fast dye generation, and very slow recombination with some inorganic semiconductors such as  $\text{TiO}_2$ .

Because of  $\text{Ag}_3\text{PO}_4$  stability and moderate bandgap that allows absorption of visible light, this study, was focused on the investigation of the photoactive inorganic/organic interface [IOI] consists of  $\text{Ag}_3\text{PO}_4$ / poly 2,2 bithiophene [PBTh] in connection with TPGE made of polyethylene glycol containing  $\text{I}^-/\text{I}_3^-$  redox system. Poly 2,2 bithiophene [PBTh] is a p-type semiconductor that has a closer bandgap to that of  $\text{Ag}_3\text{PO}_4$ .

The goal of this study is to explore the effect/s that the occlusion of  $\text{Ag}_3\text{PO}_4$  in PBTh may cause on the behavior of PBTh in this n/p junction photoactive IOI in a polymer gel electrolyte. Photoelectrochemical and impedance measurements were utilized in this study.

## 2. EXPERIMENTAL

### 2.1. Reagents

We used the monomer 2,2-bithiophene (BTh) (Alfa Aesar) to prepare poly 2,2 bithiophene [PBTh].  $\text{Ag}_3\text{PO}_4$ , PC (propylene carbonate), PEG (Polyethylene glycole), and other chemicals used in this study were of analytical grade.

### 2.2 Preparation of thermoplastic gel electrolyte [TPGE]:

Thermoplastic gel electrolyte [TPGE] was prepared following the published procedure [19]. Briefly, 0.65M KI and 0.065M  $\text{I}_2$  were dissolved in 10 mL PC, and then 8.5 g of PEG (M-20,000) was added to the mixture (PEG/KI/ $\text{I}_2$ ). The mixture was heated at 100 °C under continuous stirring for ca.

12 h in a flask under an inert atmosphere. The mixture was treated at 180 °C for 14 h in a Teflon autoclave for hydrothermal treatment.

### 2.3. Immobilization of $Ag_3PO_4$ in PBTh by occlusion method.

Particles of  $Ag_3PO_4$  were immobilized into PBTh using the electrochemical method involving the repetitive cycling of the FTO electrode potential in the suspension of  $Ag_3PO_4$  in acetonitrile solution containing 2,2-bithiophene monomer and  $LiClO_4$  was between -0.5 to 1.7 V vs Ag/AgCl. Particles of  $Ag_3PO_4$  were trapped into the polymer matrix during the polymerization process.

### 2.4. Reference electrode used in TPGE.

Because we used FTO/Pt [platinized FTO] as both counter and reference electrode in all electrochemical studies made in the electrochemical cell shown in Figure 1, all potentials measured should be vs FTO/Pt as a reference electrode. We measured this value to be 0.597V vs SHE.

### 2.5. Instrumentation

Electropolymerizations were performed in a 20 cm<sup>3</sup> three-electrode cell, consisting of a Pt flag as a counter electrode, an Ag/AgCl as reference electrode, and FTO with a surface area of 2.0 cm<sup>2</sup> as the working electrode [12]. Photoelectrochemical studies of the thin solid films were performed using the experimental setup as described in Figure 1. The working electrode is FTO covered with the photoactive polymer assembly created as described in a previous publication [12]. The gel electrolyte was poured on the surface of the working electrode and the counter electrode was pressed on the top of the gel electrolyte to make a uniform electrolyte thickness of 10 μm. Absorption spectra were performed using UVVIS EZ 2000. The electrochemical impedance spectroscopy [EIS] studies were performed using a Solartron 2101A. A BAS100W electrochemical analyzer (Bioanalytical Co. IN) was used to perform the electrochemical studies. A solar simulator 300-watt xenon lamp with an IR filter (Olympus BX-FL, Newport, NJ) was used as an illumination source. All measurements were performed at 298 °K.

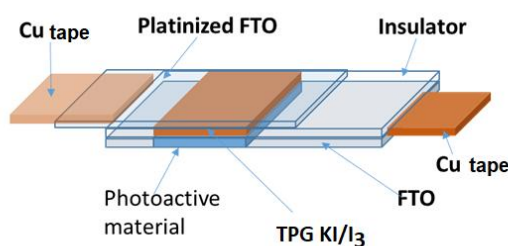


**Figure 1.** Photoelectrochemical cell-based thermoplastic Gel electrolyte (TPGE).

### 3. RESULTS AND DISCUSSION

#### 3.1 Optical band gap studies:

Figure 2A displays the absorption spectra for PBTh[a], PBTh/Ag<sub>3</sub>PO<sub>4</sub> [b] and Ag<sub>3</sub>PO<sub>4</sub> [c] assemblies. This figure indicates that the absorption spectra of Ag<sub>3</sub>PO<sub>4</sub> [c] reflect a wide absorption range, with a max absorption at around 3.5 eV. The absorption spectra of PBTh (a), and PBTh/Ag<sub>3</sub>PO<sub>4</sub> (b) show a closer band structure, and the absorption curve for PBTh/Ag<sub>3</sub>PO<sub>4</sub> shows greater light absorption for radiation with a photon energy between 3.5 to 4 eV. This can be attributed to the occlusion of Ag<sub>3</sub>PO<sub>4</sub> into PBTh. The greater absorption peak in the range of photon energies between 2.5 eV and 3 eV photon energies is due to PBTh. Figures 2B and C were prepared after-treatment of the absorption data in Figure 2 A, as plots of  $\alpha^{1/2}$  vs photon energy [hv] and  $[\alpha \cdot hv]^2$  vs hv respectively as described in previous studies [20]. Figures 2B and C indicate the existence of both direct and indirect band gaps in the studies assemblies. This is because the occlusion of Ag<sub>3</sub>PO<sub>4</sub> in PBTh created hybrid sub-bands with smaller band gaps between the highest occupied molecular orbitals [HOMO] and lowest unoccupied molecular orbitals [LUMO] of the host polymer.

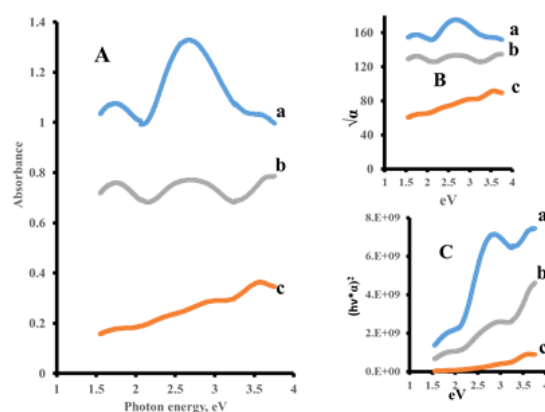


**Figure 2.** A) Absorption spectra of a) PBTh, b) PBTh/Ag<sub>3</sub>PO<sub>4</sub>, c) Ag<sub>3</sub>PO<sub>4</sub>, B)  $\alpha^{1/2}$  [cm<sup>-1/2</sup>] vs photon energy C)  $[\alpha \cdot hv]^2$ , [eV.cm]<sup>2</sup> vs photon energy

#### 3.2. Electrochemical studies in TPGE:

All electrochemical studies performed in gel electrolyte took place in electrochemical cell described in Figure 1, where the modified FTO with either PBTH or Ag<sub>3</sub>PO<sub>4</sub> or both act as working electrode, thermoplastic KI/I<sub>3</sub><sup>-</sup> gel act as an electrolyte, and FTO/Pt act as both counter and reference electrode.

##### 3.2.1 Electrochemical studies on FTO/Ag<sub>3</sub>PO<sub>4</sub>/TPGE:

The electrochemical studies on FTO/modified with previously mentioned assemblies were achieved by cycling the potential of FTO modified with each of these assemblies in the thermoplastic

KI/I<sub>3</sub><sup>-</sup> gel electrolyte [TPGE]. The studies were performed in the dark and under illumination, with a scan rate of 0.10V/s, between -1.0 to 1.6 V unless otherwise stated. The chronoamperometric studies were also performed at -0.80 V. The results are displayed in Figures 3 A, B, and C.

Figure 3A displays the CV of Ag<sub>3</sub>PO<sub>4</sub> immobilized over FTO film in KI/I<sub>3</sub><sup>-</sup> gel electrolyte in the dark and under illumination. This figure indicates that upon illumination, the Ag<sub>3</sub>PO<sub>4</sub> film shows great photocurrent, in both the cathodic and anodic scans. Such photo activities increased by increasing the illumination cycles (Figure 3A traces b, c, and d). Such increase can be attributed to the formation of Ag atoms, and further formation of another photoactive AgI (bandgap 2,58 eV) phase at the interface. The contribution of phosphate anions to this photoactivity enhancement is another factor (forthcoming in conclusion). Because the photocurrent is a direct result of charge separation and transfer, therefore the observed higher photocurrent than that observed in the absences of illumination, indicates that films of FTO/Ag<sub>3</sub>PO<sub>4</sub>/Gel electrolyte assembly, offered great charge separation and less charge recombination. Figure 3B displays the chronoamperometric studies at -0.800 V vs Ag/. The gradual increase in photocurrent and the lack of sudden photocurrent rise indicate that the FTO/Ag<sub>3</sub>PO<sub>4</sub> interface did not generate hole accumulation. Furthermore, under-dark, no sudden drop in the measured current, instead some gradual drop took place for ≈100 s ( Shaded are b, and c in Figure 3 B). Such current generated in absence of incident light photons is known as dark current, which may reflect the random generation of electrons and holes within the depletion region at the interface. Figure 3B also shows that such behavior is reproducible with less photocurrent generation. The decrease in the photocurrent in the consecutive trial can be related to the stability of the Ag<sub>3</sub>PO<sub>4</sub> film. The plot of Voc for FTO/Ag<sub>3</sub>PO<sub>4</sub>/KI/I<sub>3</sub><sup>-</sup> gel electrolyte was recorded, displayed in Figure 3 C. This figure shows that a sudden big change in the Voc during dark/illumination transitions. The following equation relates τ<sub>n</sub> with the open circuit potential (V<sub>oc</sub>) decay [21].

$$\tau_n = - [k_B T / e] * [dV_{oc} / dt]^{-1} \quad 1$$

Where k<sub>B</sub> is the Boltzmann constant, e is the electron charge, T is the temperature in K, and V<sub>oc</sub> is the open circuit potential in Volts. Applying the obtained values of The dV<sub>oc</sub>/dt in this equation, we can determine the approximate electron lifetime(τ<sub>n</sub>). The dV<sub>oc</sub>/dt = 0.415V/s. These data are corresponding to (τ<sub>n</sub>) =61 ms. This quantity is twice that calculated from Bode's plot (32 ms).

### 3.2.2 Electrochemical studies on FTO/Ag<sub>3</sub>PO<sub>4</sub>/PBTh/ /TPGE:

Figure 4A displays the CV of FTO/Ag<sub>3</sub>PO<sub>4</sub>/PBTh assembly in KI/I<sub>3</sub><sup>-</sup> gel electrolyte runs in dark and under illumination with the potential range between 0.6 V to -1.0 V. it is quite clear that the current recorded under illumination tangibly exceeds that recorded under dark in both cathodic and anodic scan. Such photocurrent is less than that recorded in Figure 3 A.

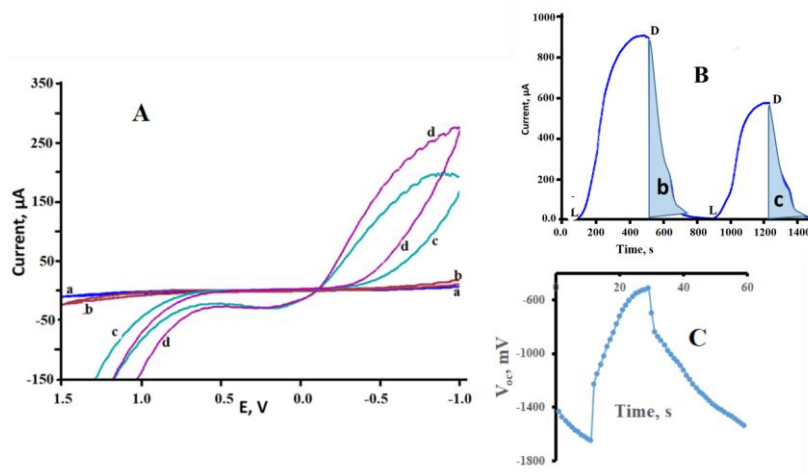


**Figure 3.** A) CV vs platinumized FTO at scan rate 0.1V/s, for  $\text{Ag}_3\text{PO}_4/\text{KI}/\text{I}_3^-$  gel electrolyte, B) photocurrent -time plot at -0.8 V, and C)  $V_{oc}$  potential vs time. a) Dark, b) 1<sup>st</sup> illumination, c) after illumination for 2 minutes, and d) after illumination for 5 minutes.

The less reported photocurrent for FTO/ $\text{Ag}_3\text{PO}_4$ /PBTh than that for FTO/ $\text{Ag}_3\text{PO}_4$  can be related to the amount of  $\text{Ag}_3\text{PO}_4$  occluded in PBTh. The photocurrent increases by applying potential that is more negative than 0.3 V, it also increases by applying potential that is more positive than 0.3 V. The photo activities of this inorganic/organic interface depend on how the valance band (VB) and conduction band (CB) in  $\text{Ag}_3\text{PO}_4$  are coordinated with the height occupied molecular orbitals (HOMO) and lowest unoccupied molecular orbitals (LUMO) of PBTh. Such coordination results in the creation of interfacial sub-bands that regulate charge separation and transfer. Similar behavior was observed in previous work [12] involved PBTh and  $\text{TiO}_2/\text{CdS}$ .

Figure 4B is a plot of photocurrent vs time (chronoamperometric) studies at -0.800 V. This figure shows that upon illumination, an initial sudden increase is followed by a gradual increase in photocurrent before it becomes steady. The figure also shows a sudden drop in the current under the dark. The absence of dark current may be attributed to the presence of PBTh that regulates the e/hole generations, and to the creation of an interfacial sub-band. The gradual increase in photocurrent may be attributed to the thermal effects of the illumination of the gel electrolytes. The initial sudden increase is attributed to that hole depletion in the p-side is less than electron depletion on the n-part of the assembly at this inorganic /organic interface (forthcoming discussion). Figure 4B also shows that such behavior is reproducible with less photocurrent generation. The decrease in the photocurrent in the second trial is related to the stability of the  $\text{Ag}_3\text{PO}_4$  /PBTh film. The plot of  $V_{oc}$  for FTO/  $\text{Ag}_3\text{PO}_4$  /  $\text{KI}/\text{I}_3^-$  gel electrolyte is displayed in Figure 4C. This figure shows that a sudden big change in the  $V_{oc}$  during dark/illumination transitions. The highest change in  $V_{oc}$  upon illumination ( $dV_{oc}/dt$ ) was 0.247 V/s. By applying Equation 1, the approximate electron lifetime ( $\tau_n$ ) is 104 ms, which indicates that the occlusion of  $\text{Ag}_3\text{PO}_4$  in PBTh elongated the electron lifetime ( $\tau_n$ ).

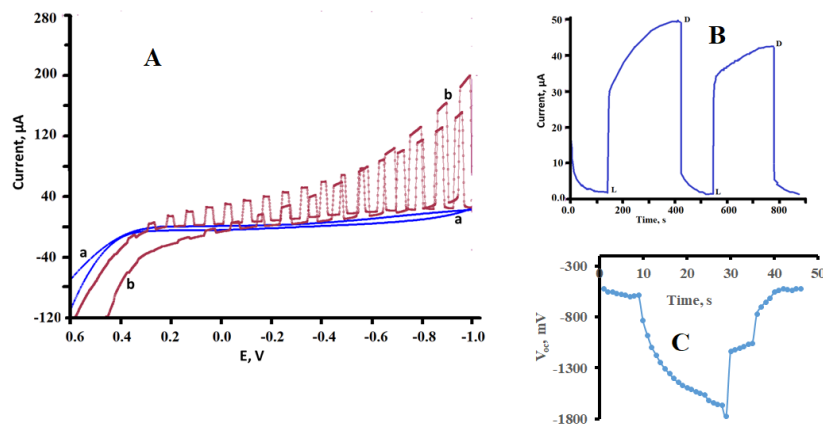


**Figure 4.** A) CV vs platinumized FTO, at scan rate 0.1V/s, for  $\text{Ag}_3\text{PO}_4/\text{PBTh}/\text{KI}/\text{I}_3^-$  gel electrolyte B) photocurrent –Time plot at -0.8 V and C)  $V_{oc}$  potential vs time. a) dark and b) illumination,

### 3.2.3 Electrochemical studies on FTO/ PBTh/ /TPGE:

Figure 5A displays the CV of FTO/ PBTh assembly in  $\text{KI}/\text{I}_3^-$  gel electrolyte runs in dark and under illumination with the potential range between 1.5 V to -1.0 V. The photocurrent current is recorded under illumination exceeds that recorded under dark at 0.6 v vs FTO/Pt. Such photocurrent is less than that recorded in Figures 3 A and 4A. This indicates that the inorganic  $\text{FTO}/\text{Ag}_3\text{PO}_4$  produced the highest photocurrent.

Figure 5B shows that upon illumination, an initial sudden increase is followed by a gradual increase in photocurrent before it becomes steady. Unlike Figure 3B, the phenomena of dark current were lacking. Figure 5B also shows that such behavior is reproducible without a loss in photocurrent generation.

Figure 5C displays the plot of  $V_{oc}$  for FTO/ PBTh/  $\text{KI}/\text{I}_3^-$  gel electrolyte vs. time. The greatest change in  $V_{oc}$  upon illumination ( $dV_{oc}/dt$ ) was 1.730 V/s. Calculation based on Equation 1, shows that the approximate electron lifetime  $[\tau_n]$  is 14 ms. This indicates that the assembly FTO/PBTh  $\text{KI}/\text{I}_3^-$  gel electrolyte generated the shortest electron lifetime ( $\tau_n$ ).

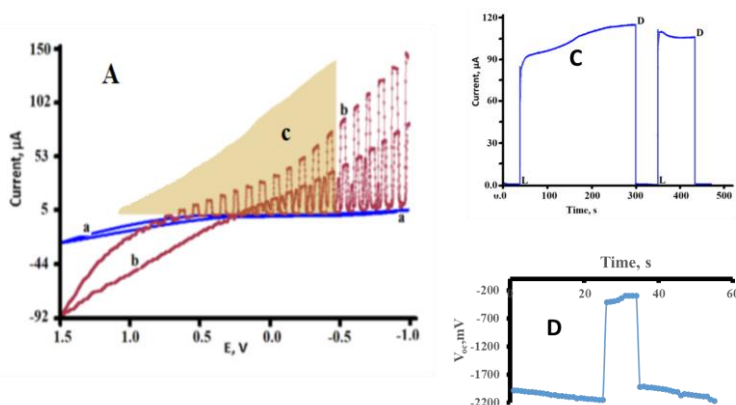


**Figure 5.** A) CV vs platinumized FTO at scan rate 0.1V/s, for PBTh/  $\text{KI}/\text{I}_3^-$  gel electrolyte, (the yellow shaded area c, is the imaginary CV vs SHE), B) Photocurrent -time plot at -0.8 V and C)  $V_{oc}$  potential vs time. a) dark and b) illumination,

Figure 6 illustrates the relative position of HOMO/LUMO and Fermi level  $E_{fb}$  [flat band potential] in both vacuum and electrochemical scales. This figure shows the increase of photocurrent at potential more negative to the  $E_{fb}$ . The CV displayed in Figure 6 also represents the electrode chemical capacitance or density of state [DoS] of PBTh assemblies at FTO. The following equation [22] was used to calculate the DoS from CV data.

$$p(E) = \frac{1}{eAd} \int \frac{idE}{s} \quad 2$$

The DoS within the potential range between 0.8 to -1.0 V shown in Figure 6 were obtained.

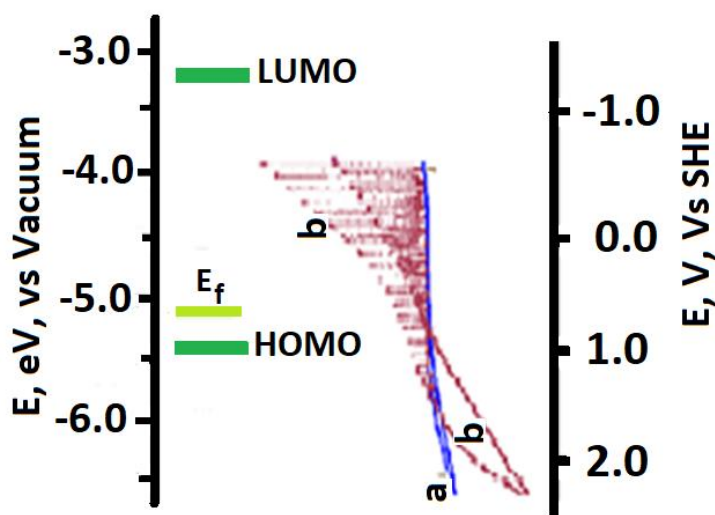


**Figure 6.** Energy diagram showing DoS and relative positions of HOMO, LUMO, and  $E_{fb}$ , of PBTh /Gel electrolyte in connection to its CV in dark/illumination, a) Dark, and b) Illumination

### 3.3.1 Electrochemical Impedance Spectroscopy [EIS] :

EIS is very effective in differentiating between different materials that possess different physical and chemical nature. In our current study, we handle an [OSC] organic semiconductor [PBTh] occluded with  $Ag_3PO_4$  as an inorganic semiconductor [ISC]. OSC exhibits amorphous, chaotic non-crystalline arrangements where charge carrier transport takes place by hopping. This will be echoed on their measured dielectric properties. On the other hand,  $Ag_3PO_4$  is an ISC band transport [ballistic conduction] where conduction is achieved by the unimpeded flow of charge carriers over a long distance in the ISC.

Impedance spectra of the assemblies were measured between  $10^5$  - $10^{-2}$  Hz. Impedance complexes [Nyquist plot], as well as other dielectric properties generated from the assemblies on FTO substrate in the dark and under illumination, are displayed in Figures 7, 8, and 9. These figures show both kinetic and diffusional control across the studied frequency range. The shape of an un-centered semicircle at high frequencies and the existence of Warburg impedance reflects the film porosity [23]. The dielectric behavior of the generated assemblies was explored at 25°C, by further treatment of EIS

data for each of the assemblies. We calculated the AC conductivities [ $\sigma_{ac}$ ] of these assemblies using the following equation [24]:

$$\sigma_{ac} = \frac{L}{a} * \frac{Z'}{Z'^2 + Z''^2} \tag{3}$$

Where L is film thickness, and an electrode surface area [2.cm<sup>2</sup>]

The other parameters such as barrier energy [ $W_m$ ], hopping frequency [ $\omega_{\text{hopping}}$ ], relaxation time [ $\tau$  in seconds ], exponent [s], and hopping distance [R] were calculated from impedance data collected under illumination and dark as previously described [12]. Table1 summarizes the quantity of s,  $W_m$ ,  $\omega_{\text{hopping}}$ ,  $\tau$  and R for FTO/PBTh, FTO/ PBTh/ Ag<sub>3</sub>PO<sub>4</sub>, and FTO/Ag<sub>3</sub>PO<sub>4</sub> as polycrystalline and amorphous photoactive materials.

**Table 1.** Exponent (s), Barrier energy ( $W_m$ ), hopping frequency ( $\omega_{\text{hopping}}$ ), relaxation time ( $\tau$ ), and hopping distance @ for the studied assemblies in KI/I<sub>3</sub><sup>-</sup> gel electrolyte at -0.800V.

Phase	Light					Dark				
	s <sup>a</sup>	$W_m$ , (eV)	$\omega$ , (KHz)	$\tau$ (mS)	R, (nm)	s	$W_m$ , (eV)	$\omega$ , (KHz)	$\tau$ (mS)	R, (nm)
PBTh	0.743	0.600	1.585	252	1.5	0.71	0.515	2.24	200	1.7
PBTh/Ag <sub>3</sub> PO <sub>4</sub>	0.565	0.354	5.62	634	2.1	0.62	0.406	3.98	200	1.8
Ag <sub>3</sub> PO <sub>4</sub>	0.446	0.278	0.148	200	3.2	0.48	0.289	0.045	80	3.1

a, the exponent in equation [power-law]  $\sigma_{ac} = \sigma_{dc} + A \omega^s$

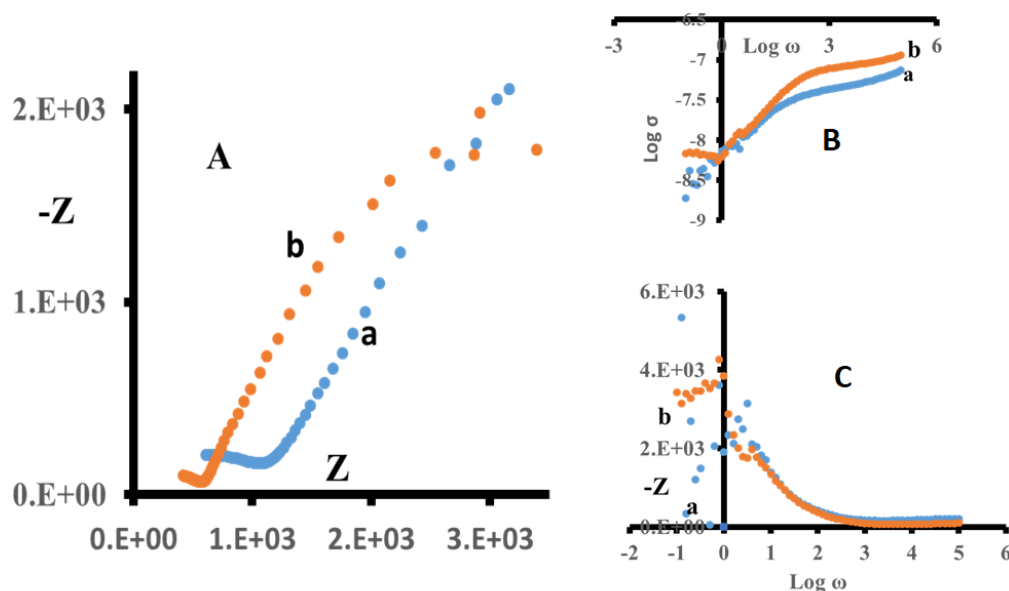


**Figure 7.** EIS at -0.80 V, for Ag<sub>3</sub>PO<sub>4</sub> assembly in KI/I<sub>3</sub><sup>-</sup> gel electrolyte, (As prepared) A) Nyquist Plot B) log conductivity  $\sigma$  vs log frequency, C) Bode's plot a] dark b] illumination

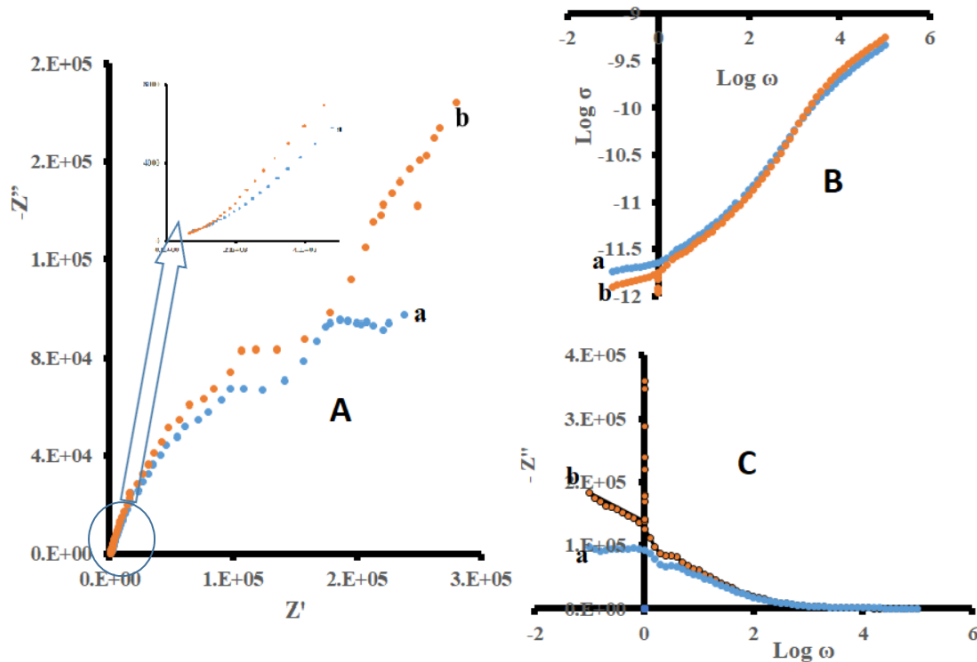


**Figure 8.** EIS at -0.80 V for FTO/PBTh in  $KI/I_3^-$  gel electrolyte, (As prepared) A) Nyquist Plot, B) log conductivity  $\sigma$  vs log frequency, C) Bode's plot a) dark b) illumination

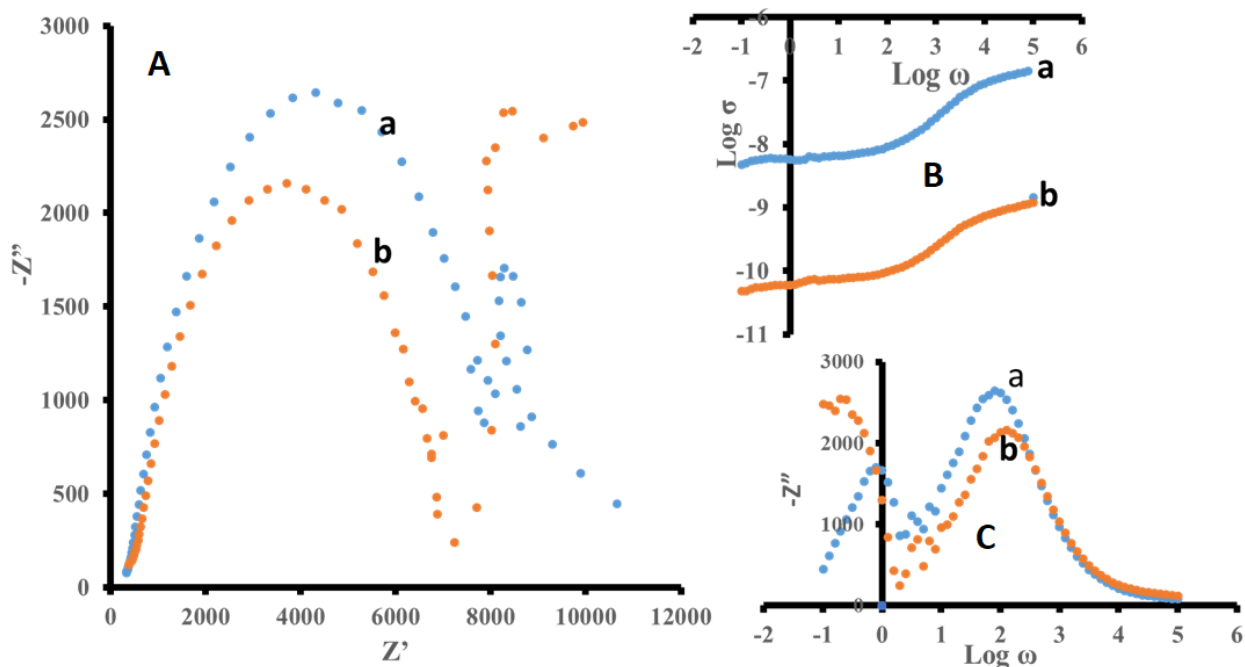


**Figure 9.** EIS at -0.80 V for  $Ag_3PO_4/PBTh$  assembly in  $KI/I_3^-$  gel electrolyte, A) Nyquist Plot B) log conductivity  $\sigma$  vs log frequency, C) Bode's plot a) dark b) illumination

The EIS studies for PBTh,  $Ag_3PO_4$ , and PBTh/  $Ag_3PO_4$  displayed in Figures 7, 8, and 9 have some common features, such as:

1- They show a composite shape results from overlapped semicircles. This composite shape semicircles at high frequency [low impedance], relate to FTO/photoactive interface, while the other portion at low frequency [high impedance] is due to anion transfer between photoactive materials and the gel polymer electrolyte. This also reflects two or more, very similar time constants.

2- The lack of intercept of the semicircle at high frequency. To have zero imaginary impedance at high frequency, the resistance should be the only component in the measured impedance. However, in the Nyquist plot, every point is the function of a complex contribution of R [true resistance], L [induction], and C [capacitance]. While L and C are dependent on frequency, R is independent of frequency. At high frequency, L is very large, or induction is very large, while the contribution of C would get very small or none at  $\infty$ . The lack of the semicircle intercept at high frequency [under the applied potential ca -0.800 V, can be attributed to the high induction effect. This accounts for the high imaginary value at high frequency.

A closer look at the data listed in table 1, shows that occlusion of  $\text{Ag}_3\text{PO}_4$  in PBTh lowered the values of s than its value in a pure PBTh. The relation between s and  $W_m$  is indicated in the following equation [25]:

$$W_m = \frac{6k_B T}{1-s} \quad 4$$

This equation shows that the greater the s the greater the carrier binding energy. The relationship [24] between R and  $W_m$  is :

$$R = \frac{2 e^2}{\pi \epsilon \epsilon_0 W_m} \quad 5$$

This means the greater the  $W_m$  the smaller the R. The values of R, listed in Table 1 are all greater than 1. This is consistent with amorphous, non-crystalline assemblies, where charge carrier transport takes place by hopping transport. The hopping mechanism takes place by either electrons transfer between localized sites or ions being tunneled to overcome the potential barriers. The hopping distance increased when  $\text{Ag}_3\text{PO}_4$  is occluded into PBTh, and reached the maximum with  $\text{Ag}_3\text{PO}_4$  assembly under dark and illumination. Regarding the relaxation time, it increases for all assemblies under illumination. The light increases dipole, ionic and dielectric relaxations. The chemical surrounding created by the occlusion of  $\text{Ag}_3\text{PO}_4$  in PBTh increased the relaxation time, although the relaxation time was the lowest in  $\text{Ag}_3\text{PO}_4$  assembly. While Ionic relaxation involves ionic conductivity at low frequencies [ca 100 Hz], The studied assemblies involved PBTh, PBTh/ $\text{Ag}_3\text{PO}_4$ , and  $\text{Ag}_3\text{PO}_4$  may encompass these types of relaxations.

### 3.3.2 Role of Ag and Orthophosphate Ions:

For the PBTh/ $\text{Ag}_3\text{PO}_4$  as p-n heterojunction assembly, the calculated work function [ $\phi$ ] for  $\text{Ag}_3\text{PO}_4$  and PBTh is 4.9 eV and 5.30 eV respectively. Under these conditions where  $\phi_p$  is  $> \phi_n$ , the creation of depletion-type heterojunction is possible. At this anisotype heterojunction, the electrons/hole concurrently accumulated and depleted on both sides of the interface [26].

The increase of photocurrent [aforementioned Figure 4A, compared to that in Figure 5A] due to the occlusion of  $\text{Ag}_3\text{PO}_4$  can be attributed to two factors;

- Ag ion effect:  $\text{Ag}^+$  can be reduced to metallic silver and PBTh becomes doped with metallic centers [27], further, it is more likely that AgI is formed at the interface between the TPGE and the assembly due to the greater solubility of  $\text{Ag}_3\text{PO}_4$  than that of AgI [bandgap 2.58 eV], that can increase light photons absorption efficiency.

- Phosphate anion effect: to the presence of phosphate anion in the studied assemblies. Phosphate is an inorganic non-metal and redox-inert anion is known for its ability to improve photocatalytic degradation of organic pollutants. Strong adsorption onto the surfaces of  $\text{TiO}_2$  by substituting surface hydroxyl groups, greatly influencing the interfacial and surface chemistry of  $\text{TiO}_2$  has been reported [28,29]. Further, the calculated electron-lifetimes for the studied assemblies were 14ms, 61 ms, and 104 ms for PBTh,  $\text{Ag}_3\text{PO}_4$ , and PBTh/ $\text{Ag}_3\text{PO}_4$  respectively. Increasing an electron lifetime in photoactive assembly is an indication of enhancement of the photoactivity. These data show that phosphate anions prolonged the lifetime of photogenerated charges resulting from the negative electrostatic field formed in the surface layers [30]. These facts recommend that the increases in the photoactivity of FTO/PBTh/ $\text{Ag}_3\text{PO}_4$  compared to that of FTO/PBTh only. Both  $\text{Ag}^+$  and  $\text{PO}_4^{3-}$  maintained their role even in the gel electrolyte that has proven long life cycles [31]

#### 4. CONCLUSION

The inorganic/organic interface [IOI] FTO/PBTh/ $\text{Ag}_3\text{PO}_4$  has been investigated in presence of a TPGE consisting of PEG/KI/I<sub>2</sub>. Occlusion of  $\text{Ag}_3\text{PO}_4$  in PBTh enhanced its photo-activities even in Gel polymer electrolytes and sustained such improvement for extended periods. Thermoplastic gel electrolytes are capable of providing liquid-like degrees of freedom. Such a property can be added to its other proven advantages such as longer life activities, and no safety problems.

#### ACKNOWLEDGMENT

The is work was supported by the academic affairs of Indiana University Kokomo.

#### References

1. Y. Liu, D. Yang, R. Yu, J. Qu, Y. Shi, H. Li and Z.-Z. Yu, *J. Phys. Chem. C.*, 121 (2017) 25172.
2. H. Fu, S. Zhang, T. Xu, Y. Zhu, and J. Chen, *Environ. Sci. Technol.*, 42 (2008) 2085.
3. L. Zhang, H. Zhang, H. Huang, Y. Liu, and Z. Kang, *New J. Chem.*, 36 (2012) 1541.
4. N. K. Eswar, P. C. Ramamurthy and G. Madras, *Photochem. Photobiol. Sci.*, 14 (2015) 1227.
5. P. Amornpitoksuk and S. Suwanboon, *Adv. Powder Technol.*, 25 (2014) 1026.
6. G. Li and L. Mao, *RSC Adv.*, 2 (2012) 5108.
7. J. Wan, E. Liu, J. Fan, X. Hu, L. Sun, C. Tang, Y. Yin, H. Li and Y. Hu, *Ceram. Int.*, 41 (2015) 6933.
8. Y. Chen, Q. Lu, X. Yan, Q. Mo, Y. Chen, B. Liu, L. Teng, W. Xiao, L. Ge, and Q. Wang, *Nanoscale Res. Lett.*, 11 (2016) 60.
9. X. Yang, H. Cui, Y. Li, J. Qin, R. Zhang, and H. Tang, *ACS Catal.*, 3 (2013) 363.
10. N. M. Mahani, *Adv. Nat. Sci.: Nanosci. Nanotechnol.*, 9 (2018) 035010.
11. K. K. Kasem, M. Elmasry, K. Baker, and C. Santucci, *Thin solid films*, 634 (2017) 56.
12. S. H. Osman, A. Jeffers, and K. Kasem, *Int. J. Electrochem. Sci.*, 14 (2019) 10729.
13. Singh, Rahul; Polu, Anji Reddy; Bhattacharya, B.; Rhee, Hee-Woo; Varlikli, Canan; Singh, Pramod

- K, *Renewable Sustainable Energy Rev.*, 65 (2016) 1098.
14. J.R. MacCallum, C.A. Vincent. *Polymer Electrolyte Reviews*. Elsevier: London; 1987 and 1989. 1 and 2.
  15. Y. Kato, S. Hori, T. Saito, K. Suzuki, M. Hirayama, A. Mitsui, M. Yonemura, H. Iba and R. Kanno, *Nat. Energy*, 1(2016) 16030.
  16. Zhigang Xue, Dan He, and Xiaolin Xie. *J Mater. Chem. A*, 3 (2015) 19218.
  17. S.A. Haque, E. Palomares, H.M. Upadhyaya, L. Otley, R.J. Potter, A.B. Holmes, *Chem Commun.*, (2003) 3008.
  18. J. Zhang, H. Han, S. Wu, S. Xu, Y. Yang, C. Zhou. *Solid State Ionics*, 178 (2007) 1595.
  19. H.L. Hsu, C.F. Tien, Y.T. Yang and J. Leu, *Electrochim. Acta*, 91 (2013) 208.
  20. J. Tauc, *Mater. Res. Bull.*, 3 (1968) 37.
  21. Arie Zaban, Miri Greenstien, and Juan Bisquert, *ChemPhysChem.*, 4 (2003) 859.
  22. Damian Monllor-Satoca and Roberto Gomez, *J. Phys. Chem. C.*, 117 (2008) 139.
  23. H. Kaiser K.D. Becca, and M.A. Gужahr, *Electrochim. Acta*, 21(1976) 539.
  24. J.H. Joshia, D.K. Kanchan, J.M. Joshi, H.O. Jethva. *Mater. Res. Bull.*, 93 (2017) 63.
  25. K. Funke, *Prog. Solid. State Chem.*, 22 (1993) 111.
  26. Haibo Wang, and Donghang Yan, *Asia Mater.* 2(2) (2010) 64.
  27. E. Bae, and W. Choi, *J. Phys. Chem. B.* 110 (2006) 14792.
  28. L. Lin, W. Lin, J. L. Xie, Y. X. Zhu, B. Y. Zhao and Y. C. Xie, *Appl. Catal., B*, 75 (2007) 52.
  29. L. Korosi and I. Dekany, *Colloids Surf., A*, 280 (2006) 146.
  30. Liqiang Jing, Jia Zhou, James R. Durrant, Junwang Tang, Dening Liu, and Honggang Fu, *Energy Environ. Sci.*, 5 (2012) 6552.
  31. K.K. Kasem, *Journal of Material Sciences and Chemical Engineering*, 9 (2021) 1.